Published by
NIGERIAN SOCIETY OF PHYSICAL SCIENCES
Available online @ https://journal.nsps.org.ng/index.php/jnsps

J. Nig. Soc. Phys. Sci. 4 (2022) 231–241

Journal of the Nigerian Society of Physical Sciences

Computational investigation of free convection flow inside inclined square cavities

Mariya Helen Mercy JK, Prabhakar.V*

Division of Mathematics, School of Advanced Sciences, Vellore Institute of Technology, Chennai, Tamil Nadu, India.

Abstract

The temperature and fluid profiles of flow inside tilted square cavities are analysed with two different cases of thermal boundary conditions, (1) Isothermally cold sidewalls of the cavity and the hot bottom wall kept parallel to the insulated top wall, (2) Hot left wall, cold right wall, insulated top and bottom walls. The Galerkin finite element method with penalty parameter is used to solve the nonlinear coupled system of partial differential equations governing the flow and thermal fields. The method is further used to solve the Poisson equation for stream function. The results are presented in terms of isotherms and streamlines. The Gaussian rule with the hybrid function formed from the block-pulse function and Lagrange polynomial is implemented for the evaluation of the definite integrals present in the residual equations. Attempting to affix the hybrid methods in the integration part for solving Finite Element Method (FEM) turned efficacious as the convergence is achieved for streamlines and isotherms with the existing results. The tilted square cavities with inclination angles $0^{\circ} \leq \phi \leq 90^{\circ}$ and Rayleigh number ranging between $10^3 \leq \mathrm{Ra} \leq 10^5$ for $Pr = 0.71$ (air) are investigated. The source code for the finite element analysis is written in Mathematica. The results thus obtained are found to be competent with those of COMSOL, the Software for Multiphysics Simulation.

DOI:10.46481/jnsps.2022.637

Keywords: Penalty finite element analysis, inclined square cavities, thermal distribution, fluid distortion, Mathematica, hybrid function, numerical integration, COMSOL

Article History :
Received: 04 February 2022
Received in revised form: 07 April 2022
Accepted for publication: 07 April 2022
Published: 29 May 2022

Communicated by: T. Latunde

1. Introduction

The term 'convection' is derived from the Latin *convectare*, which means to take to a place. During the transmission of heat, convection can be defined as the drift of heat energy from or to a solid because of nearby fluid in motion, in the existence of a temperature gradient. Further classified into two major types depending upon the source of the fluid motion: Forced convection, where the fluid movement happens due to an external influence, such as a fan, extractor, pump etc. It is called as a natural convection, when the fluid movement is solely due to the characteristics of the fluid between two determined points of the process. The fact that the velocity and the temperature equations are solved all together makes the study of natural convection seemingly complex. The natural convection within a cavity plays important roles in many science and engineering applications namely heat exchangers [1], solar stills [2], cooling of electric and electronic components [3], nanoscience [4]-[6], etc. Square cavity with obstacles, lid-driven, heated walls are also in the scope of the researchers [7]-[16].

Navier stokes equations governs the fluid flow, whereas the en-

*Corresponding author tel. no: +914439931239
Email address: prabhakar.v@vit.ac.in (Prabhakar.V)

ergy balance equations regulate the nature of the temperature. Among the various methods utilized to handle square cavities, FEM, a very competent method in dealing complex geometries and unstructured domains, is employed in this work. As the complexity increases, the integration process to calculate the stiffness and mass matrix becomes more complicated. The penalty finite element method [17] is involved in the nonlinear system of dimensionless governing equations of the 2D flow problem to waive the pressure constant. Two non-dimensional numbers, Prandtl number (Pr), signifying how much heat is carried away by how much fluid, transferring from one point to another and Rayleigh Number (Ra), describing the relationship between buoyancy and viscosity within the fluid, are explored for the convectional fluid flow. The tilted square cavities with inclination angles $0^{\circ} \leq \phi \leq 90^{\circ}$ and Rayleigh number ranging between $10^3 \leq \mathrm{Ra} \leq 10^5$ for $Pr = 0.71$ (air) are investigated. The Rayleigh number above 10^3 will display a distinctive change in the convective heat transfer rate as the inclination angle is increased. At $Ra = 10^3$ and $Ra = 10^5$ gives the minimum and maximum heat transfer rate as the angle increases [8]. Literature provides with various methods for solving ODEs and PDEs and differential equations are solved using block methods, step points, numerical methods, etc., [18]-[22].In common practice, Gaussian quadrature method is used for evaluating the integrals present in the finite element equations. Among the numerical methods available in the literature, a technique based on the Hybrid function approximation for solving nonlinear initial-value problems with applications to Lane-Emden type equations was suggested [23]. They made use of the properties of block-pulse functions and Lagrange interpolating polynomials to reduce the nonlinear initial-value problem to a system of non-algebraic equations to arrive at the accurate results. The same method was also used to provide accurate results for solving nonlinear integro-differential equations such as in Volterrra's population model [24] and Volterra-Fredholm equation, and also for variational problems. A comparative study of quadrature rules based on Haar wavelet and Hybrid function of block-pulse and Legendre polynomial, for finding the approximate value of the definite integrals, was made and the procedure was extended to the numerical solution of double and triple integrals with variable limits [25, 26]. It was observed that the hybrid method provides faster convergence when related to Haar Wavelet and that the orders of the block-pulse function and Legendre polynomial can be attuned to attain very precise solution. Hybrid of Block-Pulse function using Lagrange polynomial was considered for evaluation by [27] for the evaluation of general double and triple integrals with variable limits that shows better accuracy over Haar Wavelet. Solution of variational problems are also derived using the same [28]. Variable weights are used for the study in contrast with the constant weights considered in [25].

The square cavities inclined at angles $0^{\circ} \leq \phi \leq 90^{\circ}$ are studied with the fluid ($Pr = 0.71$) flowing within a two dimensional, steady and laminar flow across the calculation domain with two different cases of thermal boundary conditions (BC),

(Case 1) Isothermally cold sidewalls of the cavity and the hot bottom wall kept parallel to the insulated top wall,

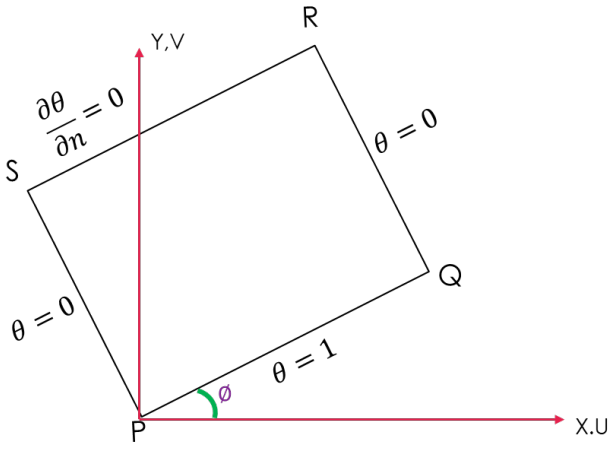

Figure 1. Square tilted at angle (Case 1) ϕ

(Case 2) Hot left wall, cold right wall, insulated top and bottom walls.

are featured in the present work. An endeavour is made to incorporate this hybrid method in the integration part for solving FEM turned efficacious as the convergence is achieved for streamlines and isotherms with the existing results in the literature [10, 12]. The source code for the finite element analysis is written in Mathematica and the results obtained are compared with COMSOL. Mathematical Procedure involving the Governing Differential Equations (GDEs) and finite element formulation is discussed in the first section, Hybrid method for the numerical integration is explained in the next section, and the results are detailed in the last section.

2. Methodology

2.1. Computational technique

The physical domain (D) of square cavity (PQRS) with angles of inclination $0^{\circ} \leq \phi \leq 90^{\circ}$ for both thermal boundary conditions is considered in the present study. The range of Rayleigh's Numbers falls between $10^3 \leq Ra \leq 10^5$ for the study. Figure 1, shows a clear picture of the geometry considered, incorporating case 1 boundary conditions.

Physical properties are kept constant during the calculation except the density in buoyancy term, where change in density due to temperature variation is estimated using Boussinesq approximation. The phenomena of thermal and fluid flow inside the domain are governed by the energy balance and Navier–Stokes equations, respectively. The governing equations for steady natural convection flow using conservation of mass, momentum and energy in dimensionless form are given below:

$$\frac{\partial U}{\partial X} + \frac{\partial V}{\partial Y} = 0 \tag{1}$$

$$U\frac{\partial U}{\partial X} + V\frac{\partial U}{\partial Y} = -\frac{\partial P}{\partial X} + \mathrm{Pr}\left(\frac{\partial^2 U}{\partial X^2} + \frac{\partial^2 U}{\partial Y^2}\right) \tag{2}$$

$$U\frac{\partial V}{\partial X} + V\frac{\partial V}{\partial Y} = -\frac{\partial P}{\partial Y} + \Pr\left(\frac{\partial^2 V}{\partial X^2} + \frac{\partial^2 V}{\partial Y^2}\right) + Ra\Pr\theta \quad (3)$$

$$U\frac{\partial \theta}{\partial X} + V\frac{\partial \theta}{\partial Y} = \frac{\partial^2 \theta}{\partial X^2} + \frac{\partial^2 \theta}{\partial Y^2} \quad (4)$$

The penalty finite element method [17] is used to eliminate the pressure term by the inclusion of the penalty parameter (γ) in the equations (2) and (3) with the following relationship involving the incompressibility.

$$P = -\gamma\left(\frac{\partial U}{\partial X} + \frac{\partial V}{\partial Y}\right) \quad (5)$$

Generally, ($\gamma = 10^7$) is considered for reliable solutions [10]. Applying (5) to (2) and (3) yields

$$U\frac{\partial U}{\partial X} + V\frac{\partial U}{\partial Y} = -\gamma\frac{\partial}{\partial X}\left(\frac{\partial U}{\partial X} + \frac{\partial V}{\partial Y}\right) + \Pr\left(\frac{\partial^2 U}{\partial X^2} + \frac{\partial^2 U}{\partial Y^2}\right) \quad (6)$$

$$U\frac{\partial V}{\partial X} + V\frac{\partial V}{\partial Y} = -\gamma\frac{\partial}{\partial Y}\left(\frac{\partial U}{\partial X} + \frac{\partial V}{\partial Y}\right) + \Pr\left(\frac{\partial^2 V}{\partial X^2} + \frac{\partial^2 V}{\partial Y^2}\right) + \mathrm{Ra}\Pr\theta \quad (7)$$

The whole domain is discretized into bi-quadratic elements. Galerkin finite element method is applied to solve the system of governing differential equations (6), (7) and (4).

A numerical integration method involving hybrid functions explained in the section 2.3 is used for obtaining the finite element solutions from the residual equations. The thermal (θ) and the velocity components ($U\&V$) are expanded through basis set $\left\{\sum_{j=1}^{9} N_j\right\}$ given in equation (8). $N_j s$ are the shape functions. The procedure to obtain $N_j s$ are detailed in [29] and those functions considered for this study is provided in the Appendix.

$$U \approx \sum_{j=1}^{9} U_j N_j(X,Y), V \approx \sum_{j=1}^{9} V_j N_j(X,Y),$$
$$\theta \approx \sum_{j=1}^{9} \theta_j N_j(X,Y) \quad (8)$$

The residual equations for an element are obtained by using (8) in the governing equations, resulting in the following system of nonlinear residual partial differential equations.

$$\begin{aligned} R_i^{(1)} &= \sum_{j=1}^{9} U_j \times \int_D \left(\left(\sum_{j=1}^{9} U_j N_j\right)\frac{\partial N_j}{\partial X} + \left(\sum_{j=1}^{9} V_j N_j\right)\frac{\partial N_j}{\partial Y}\right) N_i dXdY \\ &+ \gamma\left(\sum_{j=1}^{9} U_j \int_D \frac{\partial N_i}{\partial X}\frac{\partial N_j}{\partial X} dXdY + \sum_{j=1}^{9} V_j \int_D \frac{\partial N_i}{\partial X}\frac{\partial N_j}{\partial Y} dXdY\right) \\ &+ Pr\sum_{j=1}^{9} U_j \int_D \left(\frac{\partial N_i}{\partial X}\frac{\partial N_j}{\partial X} + \frac{\partial N_i}{\partial Y}\frac{\partial N_j}{\partial Y}\right) dXdY \end{aligned} \quad (9)$$

$$\begin{aligned} R_i^{(2)} &= \sum_{j=1}^{9} V_j \times \int_D \left(\left(\sum_{j=1}^{9} U_j N_j\right)\frac{\partial N_j}{\partial X} + \left(\sum_{j=1}^{9} V_j N_j\right)\frac{\partial N_j}{\partial Y}\right) N_i dXdY \\ &+ \gamma\left(\sum_{j=1}^{9} U_j \int_D \frac{\partial N_i}{\partial Y}\frac{\partial N_j}{\partial X} dXdY + \sum_{j=1}^{9} V_j \int_D \frac{\partial N_i}{\partial Y}\frac{\partial N_j}{\partial Y} dXdY\right) \\ &+ Pr\sum_{j=1}^{9} V_j \int_D \left(\frac{\partial N_i}{\partial X}\frac{\partial N_j}{\partial X} + \frac{\partial N_i}{\partial Y}\frac{\partial N_j}{\partial Y}\right) dXdY \\ &- \mathrm{Ra}\Pr\sum_{j=1}^{9} \theta_j \int_D N_j dXdY \end{aligned} \quad (10)$$

$$\begin{aligned} R_i^{(3)} &= \sum_{j=1}^{9} \theta_j \times \int_D \left(\left(\sum_{j=1}^{9} U_j N_j\right)\frac{\partial N_j}{\partial X} + \left(\sum_{j=1}^{9} V_j N_j\right)\frac{\partial N_j}{\partial Y}\right) N_i dXdY \\ &+ \sum_{j=1}^{9} \theta_j \int_D \left(\frac{\partial N_i}{\partial X}\frac{\partial N_j}{\partial X} + \frac{\partial N_i}{\partial Y}\frac{\partial N_j}{\partial Y}\right) dXdY \end{aligned} \quad (11)$$

For nine-noded biquadratic element (Figure 2) with three degrees of freedom, residual equations (9) – (11) consists of 27 unknowns in 27 equations.

2.2. Stream function

The stream function is used to display the fluid flow and is acquired from velocity components U and V. The relationships between stream function, ψ and velocity components for 2D flows are

$$U = \frac{\partial \psi}{\partial Y} \text{ and } V = -\frac{\partial \psi}{\partial X} \quad (12)$$

On differentiating (12), the governing equation for stream function is attained.

$$\frac{\partial^2 \psi}{\partial X^2} + \frac{\partial^2 \psi}{\partial Y^2} = \frac{\partial U}{\partial Y} - \frac{\partial V}{\partial X} \quad (13)$$

Expanding the stream function ψ using the basis set

$$\psi \approx \sum_{j=1}^{9} \psi_j N_j(X,Y) \quad (14)$$

and the relation for U, V from (8), the residual equations for (13) is,

$$\begin{aligned} R_i^{(\psi)} &= \sum_{j=1}^{9} \psi_j \int_D \left(\frac{\partial N_i}{\partial X}\frac{\partial N_j}{\partial X} + \frac{\partial N_i}{\partial Y}\frac{\partial N_j}{\partial Y}\right) dXdY - \int_\Gamma N_i n.\nabla\psi d\Gamma \\ &+ \sum_{j=1}^{9} U_j \int_D \partial N_i \frac{\partial N_j}{\partial Y} dXdY - \sum_{j=1}^{9} V_j \int_D \partial N_i \frac{\partial N_j}{\partial X} dXdY \end{aligned} \quad (15)$$

Applying no-slip boundary condition ($\psi = 0$), ψ's is obtained from the linear system (15). Stream functions ($\psi' s$) thus obtained might be positive or negative denoting the anti-clockwise and clockwise circulation respectively.

The integrands of the definite integrals appearing in (9)-(11) and (15) are functions of the global coordinates X and Y. Figure 2 shows the co-ordinate transformation for the discretized elements from the $X - Y$ plane to $s - t$ the plane [11]. The

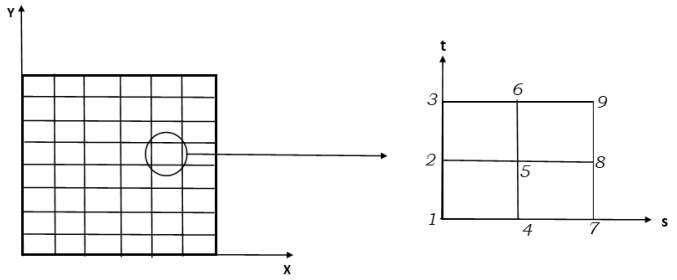

Figure 2. Coordinate transformation of the discretized element form $X - Y$ to $s - t$ plane

Table 1. Isotherms of $Ra = 10^3$; $Pr = 0.71$; PS & QR-cold; SR-adiabatic; PQ-hot

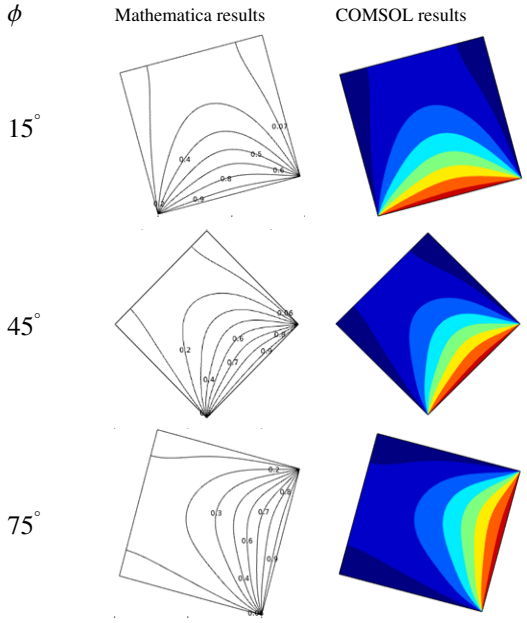

integrals appearing in the transformed residual equations are evaluated using hybrid function of block pulse function and Lagrange polynomial. The transformed residual equations solved for every node in the domain provides the thermal and velocity components. Finite element procedure to solve this is briefed in the Appendix.

It was shown that hybrid function based on block-pulse and Lagrange polynomial gives better accuracy than Haar wavelets and other hybrid functions [26], with comparatively lesser nodal points. Motivated by the accuracy of this method in solving the differential equations (both linear and nonlinear), an integration scheme based on hybrid functions for definite single, double and triple integrals was presented by [27]. An attempt has been made in applying hybrid functions to obtain the finite element solutions. Details regarding the hybrid function and the integration scheme are explained in the following section.

Table 2. Isotherms of $Ra = 10^4$; $Pr = 0.71$; PS & QR-cold; SR-adiabatic; PQ-hot

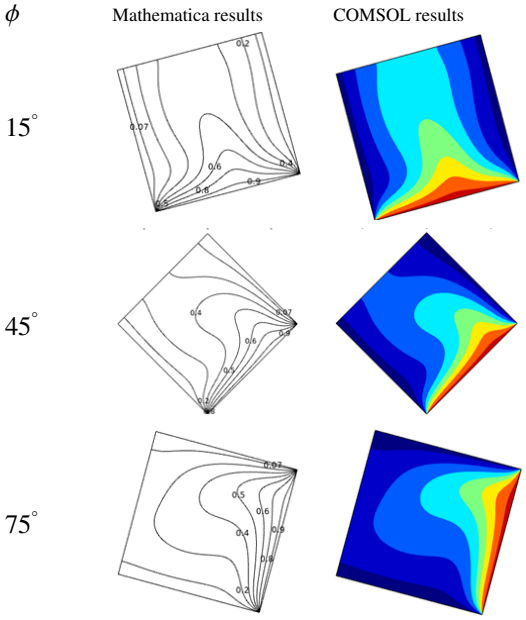

Table 3. Isotherms of $Ra = 10^5$; $Pr = 0.71$; PS & QR-cold; SR-adiabatic; PQ-hot

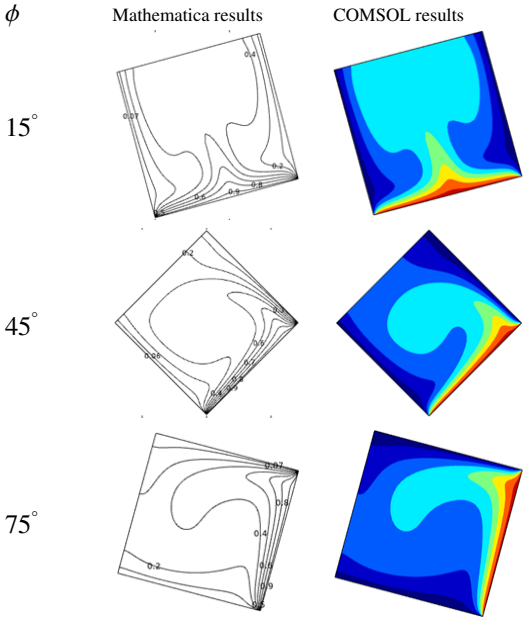

2.3. Hybrid Function

Definition 1: Block pulse functions: A set of block-pulse function $\phi_j(t), j = 1, 2, ...J$ defined on the interval $[0, 1)$ are denoted as

$$\phi_j(t) = \begin{cases} 1, & t_{j-1} \le t \le t_j \\ 0, & \text{otherwise} \end{cases} \tag{16}$$

where J represent the number of partitions of $[0, 1)$ or the order

Table 4. Streamlines of $Ra = 10^3$; $Pr = 0.71$; PS & QR-cold; SR-adiabatic; PQ-hot

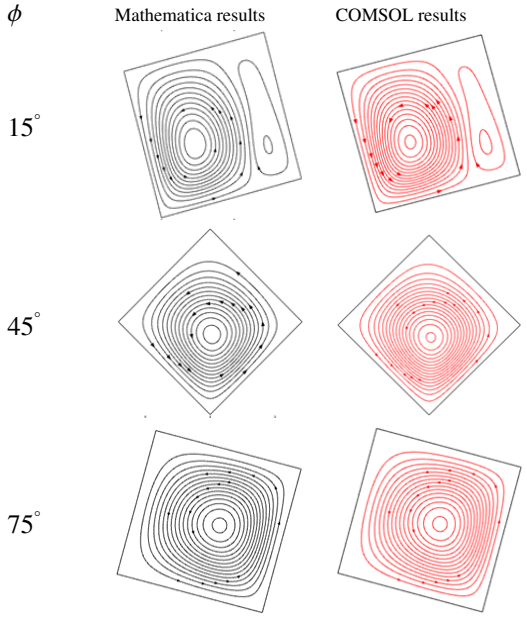

Table 5. Streamlines of $Ra = 10^4$; $Pr = 0.71$; PS & QR-cold; SR-adiabatic; PQ-hot

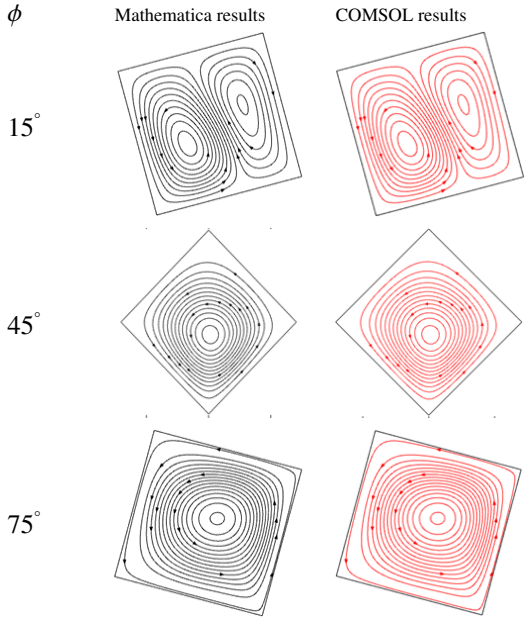

Table 6. Streamlines of $Ra = 10^5$; $Pr = 0.71$; PS & QR-cold; SR-adiabatic; PQ-hot

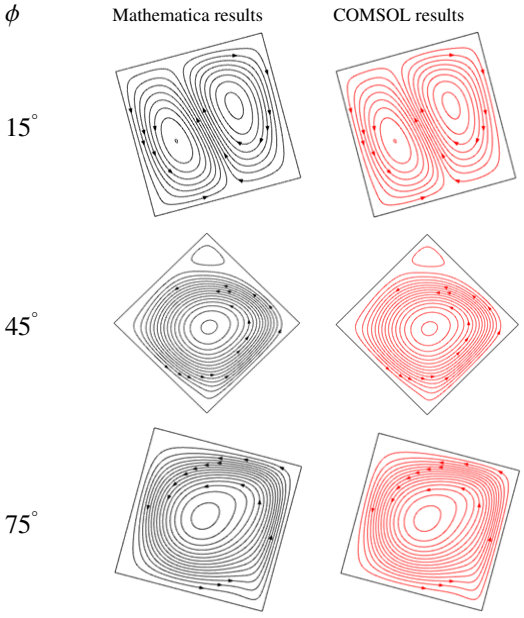

Table 7. Isotherms of $Ra = 10^3$; $Pr = 0.71$; PS-hot; QR - Cold; PQ and SR -adiabatic;

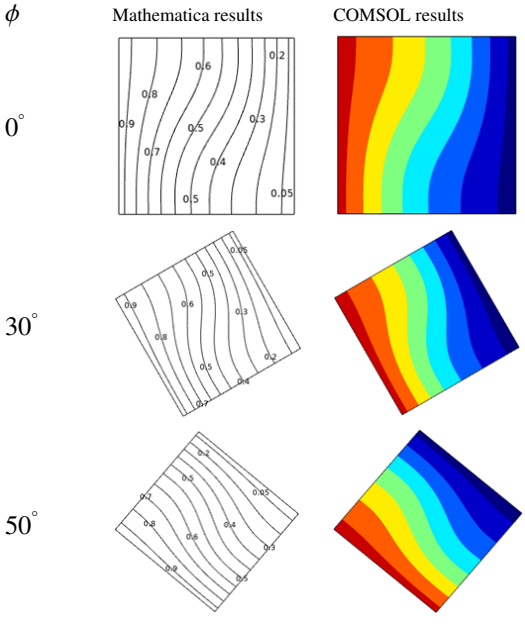

of the block pulse function in $[0, 1)$.

Definition 2: Hybrid functions of block pulse and Lagrange polynomial functions: A set of hybrid functions $h_{jk}(t), j = 1, 2, ...J$, $k = 0, 1, ...K-1$ on the interval $[0, 1)$ are denoted as

$$h_{jk}(t) = \begin{cases} L_k(2Jt - 2j + 1), & t \in \left[\frac{j-1}{J}, \frac{j}{J}\right] \\ 0, & \text{otherwise} \end{cases} \tag{17}$$

where $L_k(t)$ denoting the Lagrange polynomial of order K. As the block pulse functions and Lagrange interpolating polynomials are complete and orthogonal, $\{h_{jk}\}$ is a complete orthogonal set in the Hilbert space L^2 [23].

Table 8. Isotherms of $Ra = 10^4$; $Pr = 0.71$; PS-hot; QR - Cold; PQ and SR -adiabatic;

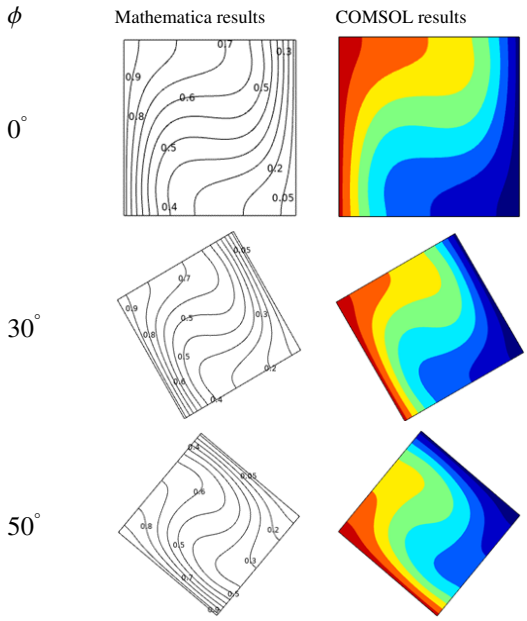

Table 9. Isotherms of $Ra = 10^5$; $Pr = 0.71$; PS-hot; QR - Cold; PQ and SR -adiabatic;

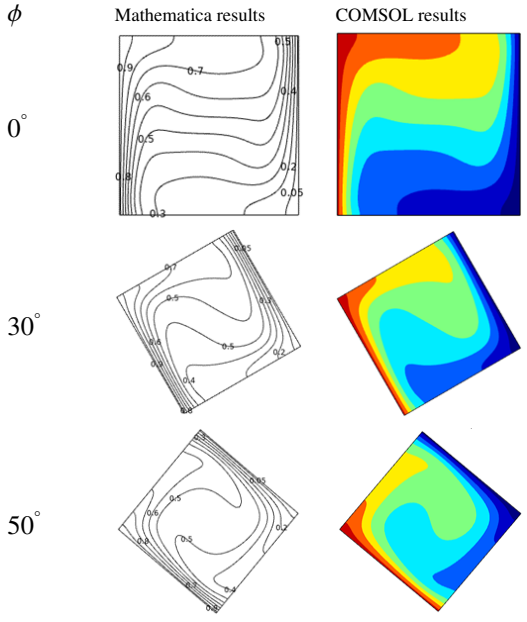

Table 10. Streamlines of $Ra = 10^3$; $Pr = 0.71$; PS-hot; QR - Cold; PQ and SR -adiabatic;

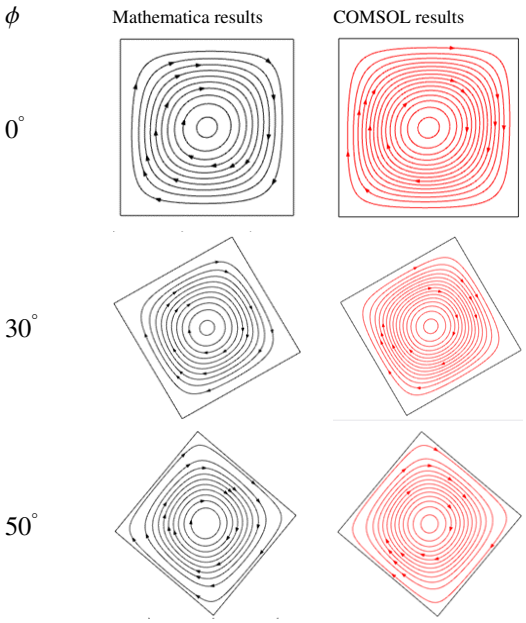

Table 11. Streamlines of $Ra = 10^4$; $Pr = 0.71$; PS-hot; QR - Cold; PQ and SR -adiabatic;

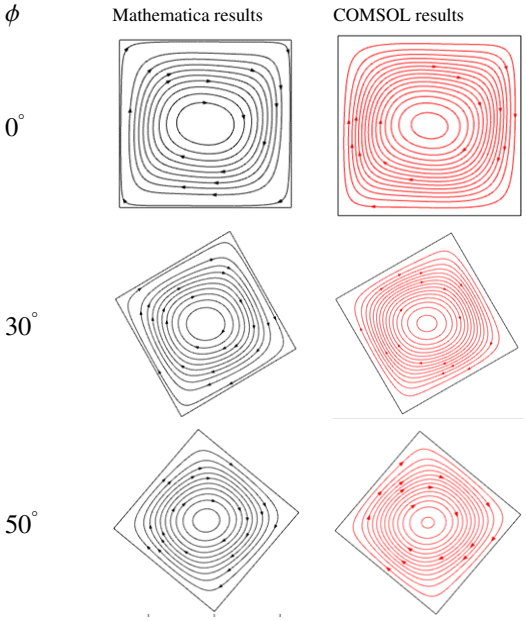

2.3.1. Approximation of function of a single variable:

A function $f(t) \in L^2\big[0,1\big)$ can be approximated, in terms of the hybrid functions as

$$f(t) = \sum_{j=1}^{\infty}\sum_{k=0}^{\infty} c_{jk} h_{jk}(t) \tag{18}$$

For an interval [0, 1) divided into J partitions and K internal nodes in each partition, $f(t)$ is taken in the form

$$f(t) \approx \sum_{j=1}^{J}\sum_{k=0}^{K-1} c_{jk} h_{jk}(t) \tag{19}$$

Considering K nodes in the j^{th} partition $\left[\frac{j-1}{J}, \frac{j}{J}\right]$, denoted by r_{jk}, it can be shown that $c_{jk} = f(r_{jk})$ [26].

Table 12. Streamlines of $Ra = 10^5$; $Pr = 0.71$; PS-hot; QR - Cold; PQ and SR -adiabatic;

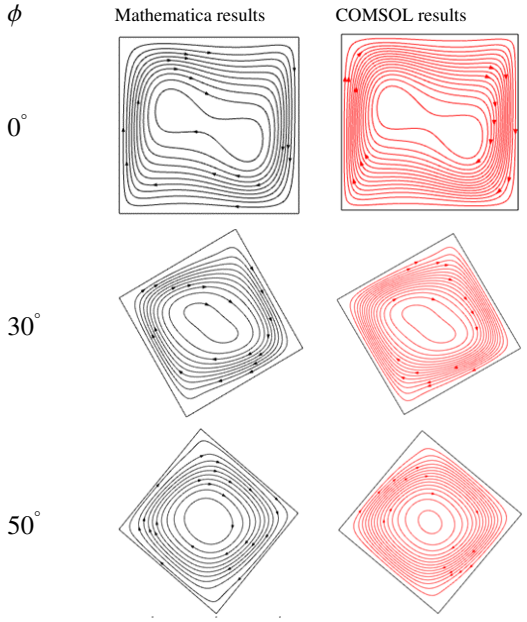

2.3.2. Approximation of function of two variables:

Extending the function approximation of a single variable in terms of hybrid functions, the function $f(t,u)$ defined in $[0,1)\times[0,1)$ can be approximated as

$$f(t,u) \approx \sum_{j=1}^{J'}\sum_{k=0}^{K'-1}\sum_{j=1}^{J}\sum_{k=0}^{K-1} c_{jklm} h_{jk}(t) h_{lm}(u) \tag{20}$$

by considering J partitions and K internal nodes in each partition for $[0,1)$ in the t-direction, and J' partitions and K' internal nodes in each partition for $[0,1)$ in the u-direction. It can be shown that

$$c_{jklm} = f\left(r_{jk}, r_{lm}\right) \tag{21}$$

where Gaussian nodes along the t and u directions are and r_{jk} and r_{lm} respectively [25].

2.3.3. Integration scheme for the integrals in residual equations:

Using the function approximation from equations (19) and (20), the integrals (both single and double) of the residual equations can be easily evaluated as follows.

$$\int_0^1 f(t)dt = \sum_{j=1}^{J}\sum_{k=0}^{K-1} c_{jk} w_{jk} \tag{22}$$

where $w_{jk} = \int_0^1 h_{jk}(t)dt$ are the weights. As the hybrid function $h_{jk}(t)$ is a polynomial, its weight can be easily calculated.

Similarly,

$$\int_0^1\int_0^1 f(t,u)dtdu = \sum_{j=1}^{J'}\sum_{k=0}^{K'-1}\sum_{j=1}^{J}\sum_{k=0}^{K-1} c_{jklm} w_{jk} w_{lm} \tag{23}$$

where $w_{jk} = \int_0^1 h_{jk}(t)dt$ and $w_{lm} = \int_0^1 h_{lm}(u)du$ are the weights. For single integral $J = 1$ and $K = 2$; for double integrals $J = 2$, $K = 4$, $J' = 3$ and $K' = 5$ are well accommodated for the integrals present in the residual equations.

3. Results and discussion

We consider a two dimensional, steady and laminar flow across the inclined square cavity (PQRS) under two different thermal boundary conditions as mentioned in section 1. The physical domain (D) of square cavity with angle of inclination (ϕ), inclined with the X-axis within the acute angles of $15^\circ, 45^\circ$ and 75° for case 1 and $0^\circ, 30^\circ$ and 50° for case 2 thermal boundary conditions is considered for the present study. $Pr = 0.7$, and Ra varied from 10^3 to 10^5 for both the boundary conditions are investigated. In order to assess the accuracy of our numerical procedure, we have tested our algorithm for the results presented in [10] for 28×28 elements and found to be exactly matching. In this paper, however, we restrict our study considering 20×20 elements (Figure 3) with the grid size of 51×51, which were also found to be in good agreement with the isotherms and streamlines reported in [10]. Distributions of isotherms and streamlines of case (1) are portrayed in Tables 1-3 and 4-6 respectively; Similarly Tables 7-9 and 10-12 illustrates the heat and fluid contours of case (2).

Observing the isotherms for case (1), when Ra is 10^3, however inclined the square cavity is, there is not much disruption, indicating heat transfer through conduction as depicted in Table 1, whereas, when Ra is increased, isotherms are concentrated at the hot and cold walls. Both clockwise and anticlockwise circulations seen in all the Rayleigh numbers are pondered at $\phi = 15^\circ$. When Ra is 10^3, the secondary cells are comparatively lesser in size but when it is 10^4 the cells are slightly bigger and when the value of Ra is 10^5 the two axisymmetric flow exquisitely occupies the entire cavity. As ϕ increases to 45° , the strength of anticlockwise circulation cells increases (Table 5). As the angle of inclination increases, there is a significant push of isotherms towards the right wall. At $\phi = 75^\circ$, the isotherms are found to be qualitatively similar to those of $\phi = 45^\circ$ as the temperature contours are piling towards the right wall (Tables 2 and 3). The overall amount of heat transfer along the right wall increases with inclination angle and decreases along the left wall.

In Table 6 at 45°, strong primary anticlockwise circulation cells occupy almost the entire part of cavity except top corner of the wall QR. As inclination angle ϕ further increases to 75°, the primary circulation cells span the entire cavity whereas secondary circulation cells completely disappear. It is interesting to observe that the centre of left vortex for the fluid

circulations is pushed towards the bottom wall and centre of right vortex is pushed towards the top wall due to enhanced tangential components of buoyancy force along the bottom wall which tends to impose an anticlockwise fluid circulation.

Exploring case (2), the temperature contours exhibit a gentle migration from left to right side of the calculation domain for all the investigated. In Table 7, dealing with the $Ra = 10^3$, the contours are observed to exhibit an elegant protuberance toward the right wall as there is a surge in the inclination angles. Streamlines in these conditions are not much varied but are laminar in nature as in Tab.12. With increase in Ra, heat transfer due to convection is clearly visible (Table 9). The difference is observed as ϕ is gradually amplified. The fluid flow is more unruffled than in the case 1. Only when $Ra = 10^5$ and $\phi = 0^\circ$, the centre of the vortex is not circular in shape as in Table 12. The flow in the circulation cells are almost circular in shape near the core and further, they swell and take the shape of the cavity near the walls due to strong convection only increasing the angle of inclination. From what is seen in the isotherms the convection mode of heat transfer dominates over the conduction, as the inclination angle increases. Evident picture of the conduction effect can be seen in the contour for temperature. The movement of fluid backs up the convection, due to the bulk movement of air triggers the convective heat transfer moves the constant temperature line in the direction of its motion.

Hence, the circulation cells are strained along these walls, prevailing in the sizeable portion of the central region. The temperature layer in the core breaks down because of the good mixing occurring in the core. The inclined square is the calculation domain, hence the effect of tangential and normal components of buoyancy force relative to hot wall gains importance for flow and thermal phenomena. Stronger anticlockwise fluid circulations are witnessed when increasing the angle of inclination as the buoyancy force along the hot wall also grows. Results indicate that the fluid circulations, isotherms are strongly dependent on the inclination angle of the square cavity. The heat and the flow contours obtained by using the hybrid function are in good agreement with [10] for case (1) and [12] for case (2) where the FEM with traditional Gaussian quadrature were used to carry out the calculation.

3.1. Comparison using COMSOL

The COMSOL Model Wizard was used to create a stationary, 2D Multiphysics model. The computation was carried out in a physical machine with Intel i7 64-bit processor with 8 GB of memory and SSD for storage, loaded with Windows 10 Operating system. The time taken for computation for a particular Pr and various Ra is 20 seconds. The 2D geometry is mathematically extended to infinity in both directions along the z-axis, assuming no variation along that $z - axis$. A square with $1metre$ on all sides is built, inclined to specific angles for needed cases. Different components with different inclination angles are created in the same model. 'Parameters' nodes are present under global definitions, that are used for creating and

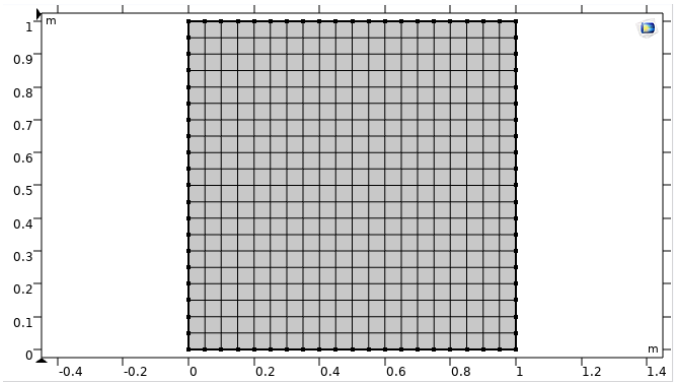

Figure 3. 20×20 meshing of the domain

defining the values of the non-dimensional temperature boundary conditions for hot, cold and adiabatic walls, Rayleigh Number, Prandtl Number and the reference pressure.

Coupling of the fields are at ease even with more than one physics interface. All applicable fields that can be used as inputs in one physics interface is spontaneously found in the other physics interface's Settings. Laminar flow (spf) takes care of fluid properties, initial conditions, volume force and the pressure of the fluid. Heat Transfer in Fluids (ht) handles the nature of the heat transfer and the temperature boundary conditions. The Mesh nodes are generated by meshing the domain, which enables the discretization of the geometry into mesh elements. The parameter Ra varied is listed for the given range using Auxiliary sweep. The set-up is computed. COMSOL Multiphysics generates plot windows for displaying convergence results and isothermal contours and streamlines. The results from COMSOL are compared with those of Mathematica for every boundary condition and Ra found to be in good agreement.

4. Conclusion

In this paper, we considered a two dimensional, steady and laminar flow across the tilted square cavity under two different thermal boundary conditions: case (1) Isothermally cold sidewalls of the cavity and the hot bottom wall kept parallel to the insulated top wall and case (2) Hot left wall, cold right wall, insulated top and bottom walls. In case 1, it is found that two axisymmetric flows dwell in the entire cavity, whereas, as the angle of inclination increases, the primary circulation cells occupy the entire cavity and the secondary circulation cells disappear completely. In case 2, only at $Ra = 10^5$, the streamlines are circular only on enlarging inclination of the square cavity. In both the cases as inclination increases, buoyancy force along the hot wall gradually increases leading to stronger anticlockwise fluid circulations corresponding to the Rayleigh number. Results indicate that the streamlines and isotherms are strongly dependent on the inclination angle of the cavity. An attempt has been made to evaluate the definite integrals of the residual equations of the finite element equations using Gaussian quadrature with Hybrid functions of block-pulse function and Lagrange polynomial as orthogonal polynomials, and the results are found

to be in accordance with [10] for case (1) and [12] for case (2). With hybrid functions, desired accuracy can be achieved with the flexibility of choosing the orders of block pulse function and Lagrange polynomial independently. Finite element results presented with Wolfram Mathematica were found to be in good agreement with COMSOL Multiphysics. The model can be applied for a field problem like plastic injection mould flow, porous media flow etc., by varying the variables such as fluid temperature, fluid velocity, mass weight and flow rate.

Acknowledgments

We thank the referees for the positive enlightening comments and suggestions, which have greatly helped us in making improvements to this paper.

APPENDIX

A.Notations used:

$X = \frac{x}{L}, Y = \frac{y}{L}$, ($X$ and Y - distance in dimensionless form)

$U = \frac{uL}{\alpha}, Y = \frac{vL}{\alpha}$, ($U$ and V - velocity components in dimensionless form)

$\theta = \frac{T - T_c}{T_h - T_c}$ (θ - temperature component in dimensionless form; T_h&T_c-Temperature at hot and cold)

$P = \frac{pL^3}{\rho\alpha^2}$ (P - pressure in the dimensionless form)

$Pr = \frac{\nu}{\alpha}$ (Pr - Prandtl number)

$Ra = \frac{g\beta(T_h - T_c)L^3 Pr}{\nu}$ (Pr - Rayleigh number)

$\alpha = \frac{k}{\rho C_p}$ (α - Thermal diffusivity)

B.The shape functions of the transformed residuals from $X - Y$ to $s - t$ plane with reference to the local numbering in the Figure 2.

$N_1 = (1 - 3s + 2s^2)(1 - 3t + 2t^2);$
$N_2 = (1 - 3s + 2s^2)(4t - 4t^2);$
$N_3 = (1 - 3s + 2s^2)(-t + 2t^2);$
$N_4 = (4s - 4s^2(1 - 3t + 2t^2);$
$N_5 = (4s - 4s^2)(4t - 4t^2);$
$N_6 = (4s - 4s^2)(-t + 2t^2);$
$N_7 = (-s + 2t^2)(1 - 3t + 2t^2);$
$N_8 = (-s + 2t^2)(4t - 4t^2);$
$N_9 = (-s + 2t^2)(-t + 2t^2);$

C.The nonlinear residual equations (9) - (11) are solved by the following procedure

Grouping the co-efficient of $\sum_{j=1}^{9} U_j$ from all three residues

$$s_{11} = \int_D \left(\left(\sum_{j=1}^{9} U_j N_j\right)\frac{\partial N_j}{\partial X} + \left(\sum_{j=1}^{9} V_j N_j\right)\frac{\partial N_j}{\partial Y}\right) N_i dXdY + \gamma \int_D \frac{\partial N_i}{\partial X}\frac{\partial N_j}{\partial X} dXdY + Pr \int_D \left(\frac{\partial N_i}{\partial X}\frac{\partial N_j}{\partial X} + \frac{\partial N_i}{\partial Y}\frac{\partial N_j}{\partial Y}\right) dXdY \tag{C.1}$$

$$s_{12} = \gamma \int_D \frac{\partial N_i}{\partial Y}\frac{\partial N_j}{\partial Y} dXdY \tag{C.2}$$

$$s_{13} = 0 \tag{C.3}$$

Grouping the co-efficient of $\sum_{j=1}^{9} V_j$ from all three residues

$$s_{21} = \gamma \int_D \frac{\partial N_i}{\partial Y}\frac{\partial N_j}{\partial X} dXdY \tag{C.4}$$

$$s_{22} = \int_D \left(\left(\sum_{j=1}^{9} U_j N_j\right)\frac{\partial N_j}{\partial X} + \left(\sum_{j=1}^{9} V_j N_j\right)\frac{\partial N_j}{\partial Y}\right) N_i dXdY + \gamma \int_D \frac{\partial N_i}{\partial Y}\frac{\partial N_j}{\partial Y} dXdY + Pr \int_D \left(\frac{\partial N_i}{\partial X}\frac{\partial N_j}{\partial X} + \frac{\partial N_i}{\partial Y}\frac{\partial N_j}{\partial Y}\right) dXdY \tag{C.5}$$

$$s_{23} = -Ra\,\mathrm{Pr} \sum_{j=1}^{9} \theta_j \int_D N_j dXdY \tag{C.6}$$

Grouping the co-efficient of $\sum_{j=1}^{9} \theta_j$ from all three residues

$$s_{31} = 0 \tag{C.7}$$

$$s_{32} = 0 \tag{C.8}$$

$$s_{33} = \int_D \left(\left(\sum_{j=1}^{9} U_j N_j\right)\frac{\partial N_j}{\partial X} + \left(\sum_{j=1}^{9} V_j N_j\right)\frac{\partial N_j}{\partial Y}\right) N_i dXdY + \int_D \left(\frac{\partial N_i}{\partial X}\frac{\partial N_j}{\partial X} + \frac{\partial N_i}{\partial Y}\frac{\partial N_j}{\partial Y}\right) dXdY \tag{C.9}$$

Rewriting the governing equations, with the above substitutions, in matrix form

$$\begin{Bmatrix} R_i^{(1)} \\ R_i^{(2)} \\ R_i^{(3)} \end{Bmatrix} = \sum_{j=1}^{9} \begin{bmatrix} s_{11}^{i,j} & s_{12}^{i,j} & s_{13}^{i,j} \\ s_{21}^{i,j} & s_{22}^{i,j} & s_{23}^{i,j} \\ s_{31}^{i,j} & s_{32}^{i,j} & s_{33}^{i,j} \end{bmatrix} \begin{Bmatrix} U_j \\ V_j \\ \theta_j \end{Bmatrix} \tag{C.10}$$

$$\left\{\overline{R_i}\right\} = \left[k_{ij}\right]\left\{\overline{U_j}\right\}, 1 \le i \le 9 \tag{C.11}$$

The integrands, which leads to the element stiffness matrix, are functions of the global coordinates X and Y. The functions N_j can be expressed in terms of the local coordinates s and t. Figure 2 gives an idea of co-ordinate transformation for the discretized elements in the $X - Y$ plane to the $s - t$ plane.

$$X = \sum_{j=1}^{9} x_j N_j \text{ and } Y = \sum_{j=1}^{9} y_j N_j \tag{C.12}$$

The integrand contains not only functions but also derivatives with respect to the global coordinates (x_j, y_j). Therefore, $\frac{\partial N_j}{\partial X}$ and $\frac{\partial N_j}{\partial Y}$ must be related to $\frac{\partial N_j}{\partial s}$ and $\frac{\partial N_j}{\partial t}$. Applying the shape functions to equation (C.10), the transformed finite element equation is obtained. Element stiffness matrices thus obtained are assembled using the element connectivity (Table 13) resulting in a global stiffness matrix.

The global stiffness matrix is solved to get the thermal and the velocity components. On applying of the boundary conditions to the walls, matrix reduces to 9 nodes (internal), i.e., 27

Table 13. Element connectivity involving Nodes (N) and Elements (E)

NE	1	2	3	4
1	1	3	11	13
2	2	4	12	14
3	3	5	13	15
4	6	8	16	18
5	7	9	17	19
6	8	10	18	20
7	11	13	21	23
8	12	14	22	24
9	13	15	23	25

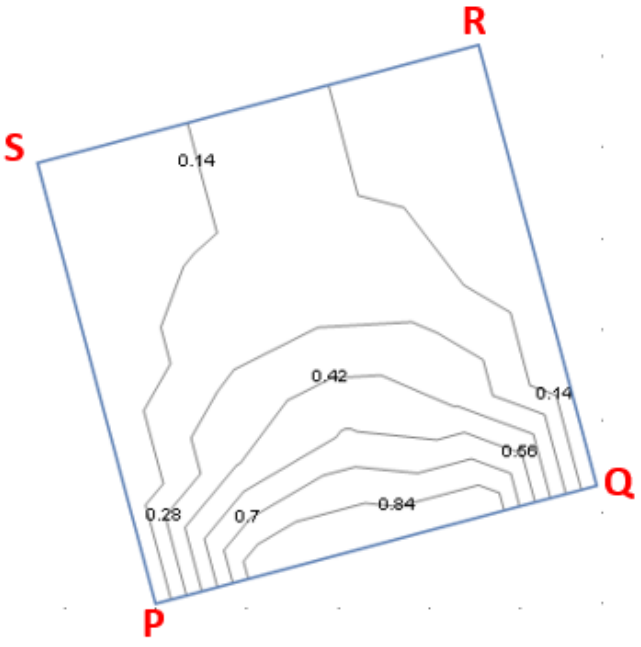

Figure 4. Isotherms contour of 4 elements inclined $\phi = 15^{\circ}$; $Ra = 10^4$; $Pr = 0.71$ obtained from Mathematica

unknowns and equations, for the entire domain discretized to for 2×2. The temperature contours of 4 elements for a tilted square cavity with $Ra = 10^4$; $Pr = 0.71$ is displayed in Figure 4.

The values of the velocity (U ,V) and thermal components (θ) for the internal nodes of the discretized domain with 2×2 (4 elements) are given below.

$U_7 = -0.0000228252, V_7 = -0.0000176029, \theta_7 = 0.414016,$
$U_8 = 4.69382\text{E-}6, V_8 = -1.88969\text{E-}6, \theta_8 = 0.208614,$
$U_9 = 0.0000131575, V_9 = -1.06333\text{E-}6, \theta_9 = 0.121948,$
$U_{12} = -0.0000119197, V_{12} = -0.000053752, \theta_{12} = 0.575621,$
$U_{13} = 0.0000149714, V_{13} = -0.0000638262, \theta_{13} = 0.271557,$
$U_{14} = 0.0000157566, V_{14} = -0.000030133, \theta_{14} = 0.171982,$
$U_{17} = 1.58957\text{E-}6, V_{17} = -0.000024564, \theta_{17} = 0.414017,$
$U_{18} = 1.69972\text{E-}6, V_{18} = -0.0000310296, \theta_{18} = 0.208615,$
$U_{19} = -1.65325\text{E-}6, V_{19} = -0.0000198665, \theta_{19} = 0.121949.$

The discretization was gradually increased until the convergence was obtained at 20×20.

References

[1] L. Viorel & N. Anisoara, "Numerical modelling of fluid flow and heat transfer in a corrugated channel for heat exchanger applications", Procedia Manufacturing **22** (2018) 634.

[2] A. Omri, J. Orfi & S.B. Nasrallah, "Natural convection effects in solar stills", Desalination **183** (2005) 73.

[3] G.D. Mey, M. Wojcik, J. Pilarski, M. Lasota, J. Banaszczyk, B. Vermeersch, A. Napieralski & M.D. Paepe, "Chimney effect on natural convection cooling of a transistor mounted on a cooling fin", Journal of Electronic Packaging **131** (2009) 14501.

[4] M. Sabour, M. Ghalambaz, & A Chamkha, "Natural convection of nanofluids in a cavity: criteria for enhancement of nanofluids",International Journal of Numerical Methods for Heat and Fluid Flow **27** (2017) 1504.

[5] K. Wisam, B.Hussama, K. Khanafera, H.J. Salema & Sheard GJ, "Natural convection heat transfer utilizing nanofluid in a cavity with a periodic side-wall temperature in the presence of a magnetic field",International Communications in Heat and Mass Transfer **104** (2019) 127.

[6] N. Nabipour, M. Babanezhad, A.T.Nakhjirin, & S. Shirazian, "Prediction of Nanofluid Temperature Inside the Cavity by Integration of Grid Partition Clustering Categorization of a Learning Structure with the Fuzzy System",International Communications in Heat and Mass Transfer **5** (2020) 3571.

[7] A.J. Chamkha, "Hydromagnetic combined convection flow in a vertical lid-driven cavity with internal generation or absorption",An International Journal of Computation and Methodology **41** (2002) 529.

[8] C.S.N. Azwadi, M.Y.M Fairus & Syhrullail.S, "Virtual Study of Natural convection Heat transfer in an Inclined square cavity",Journal of Applied Sciences **10** (2010) 331.

[9] M.K Das & K.S.K Reddy, "Conjugate natural convection heat transfer in an inclined square cavity containing a conducting block",International Journal of Heat and Mass Transfer **49** (2006) 4987.

[10] A.K. Singh, S. Roy, T. Basak, "Analysis of Bejan's heatlines on visualization of heat flow and thermal mixing in tilted square cavities",International Journal of Heat and Mass Transfer **55** (2012) 2965.

[11] J.K. Mariya Helen Mercy & V. Prabhakar, "Study of fluid flow inside closed cavities using computational numerical methods",International Journal for Simulation and Multidisciplinary Design Optimization **12** (2012) 1.

[12] J. Rasoul & P. Prinos, "Natural convection in an inclined enclosure",International Journal of Numerical Methods for Heat & Fluid Flow **12** (1997) 438.

[13] F. Xu, J.C. Patterson, C. Lei, "Natural convection in a differentially Heated cavity with a square obstruction on the sidewall",Australian Journal of Mechanical Engineering **4** (2015) 77.

[14] Bendaraa et al, "Numerical Study of Natural Convection in Square Cavity Using Lattice Boltzmann Method: Obstacles Effect", IOP Conf. Ser: Mater. Sci. Eng **948** (2020) 1.

[15] J. Vierendeels, B. Merci & E.Dick, "Benchmark solutions for the natural convective heat transfer problem in a square cavity with large horizontal temperature differences",International Journal of Numerical Methods for Heat & Fluid Flow **13** (2003) 1057.

[16] R.C. Mohapatra, "Study on Natural Convection in a Square Cavity with Wavy right vertical wall Filled with Viscous Fluid",Journal of Mechanical and Civil Engineering **14** (2017) 32.

[17] J.N. Reddy, *An Introduction to the Finite Element Method*, United States of America, McGraw-Hill, New York (1993).

[18] Victor Oboni Atabo, Solomon Ortwer Adee, "A New Special 15-Step Block Method for Solving General Fourth Order Ordinary Differential Equations",J. Nig. Soc. Phys. Sci.**3** (2021) 308.

[19] Mark I. Modebei, Olumide O. Olaiya, Ignatius P. Ngwongwo, "Computational study of a 3-step hybrid integrators for third order ordinary differential equations with shift of three off-step points",J. Nig. Soc. Phys. Sci.**3** (2021) 459.

[20] V. J. Shaalini, S. E. Fadugba, "A New Multi-Step Method for Solving Delay Differential Equations using Lagrange Interpolation",J. Nig. Soc. Phys. Sci.**3** (2021) 159.

[21] Friday Obarhua, Oluwasemire John Adegbor, "An Order Four Continuous Numerical Method for Solving General Second Order Ordinary Differential Equations",J. Nig. Soc. Phys. Sci.**3** (2021) 42.

[22] Olumide O. Olaiya, Rasaq A. Azeez, Mark I. Modebei, "Efficient Hybrid Block Method For The Numerical Solution Of Second-order Partial Differential Problems via the Method of Lines",J. Nig. Soc. Phys. Sci.**3** (2021) 26.

[23] H.R. Marzban, H.R. Tabrizidooz & M. Razzaghi, "Hybrid functions for nonlinear initial value problems with applications to Lane-Emden type equations",Physics Letters A **372** (2008) 5883.

[24] H.R. Marzban, S.M. Hoseini & M. Razzaghi, "Solution of Volterra's population model via block-pulse functions and lagrange interpolating polynomials",Math Methods Appl Sci, **32** (2009) 127.

[25] Siraj-Ul-Islam, I. Aziz & F. Haq, "A comparative study of numerical integration based on Haar wavelets and hybrid functions",Computers and Mathematics with Applications, **59** (2009) 2026.

[26] I. Aziz, Siraj-Ul-Islam, & W. Khan, "Quadrature rules for numerical integration based on haar wavelets and hybrid functions",Computers and Mathematics with Applications, **61** (2011) 2770.

[27] G. Uma, V. Prabhakar & S. Hariharan, "Numerical integration using hybrid of block-pulse functions and Lagrange polynomial",International Journal of Pure and Applied Mathematics, **106** (2016) 33.

[28] H.R. Marzban, H.R. Tabrizidooz & M.Razzaghi, "Solution of variational problems via hybrid of block-pulse and Lagrange interpolating",ET Control Theory Appl, **3** (2009) 1363.

[29] Larry J.Segerlind, *Applied finite element analysis*, United States of America, John Wiley & Sons, New York (1984).